Journal of Applied Polymer Science

Foaming of Polypropylene with Supercritical Carbon Dioxide: An Experimental and Theoretical Study on a New Process

Jie Ding, Weihua Ma, Fujiao Song, Qin Zhong
School of Chemical Engineering, Nanjing University of Science and Technology, Nanjing, Jiangsu, 210094, People's Republic of China
Correspondence to: W. Ma (E-mail: maweihuacn@yahoo.com.cn) or Q. Zhong (E-mail: zq304@mail.njust.edu.cn)

ABSTRACT: A new process was used to foam polypropylene (PP) with batch foaming technique with supercritical carbon dioxide ($scCO_2$) as the blowing agent. Comparing with the conventional process, the new one takes less time to foam and the foaming temperature range is much broader, which is about 2.5 h and 55°C, respectively. An activation model was established on the basis of mass equilibrium, this model was combined with classical nucleation theory and S-L EOS model to explain foaming behaviors of PP and simulate the cell nucleation and cell diameter. A satisfactory agreement between calculated and experimental values was obtained.
 J. Appl. Polym. Sci. 130: 2877–2885, 2013

KEYWORDS: foams; porous materials; theory and modeling

Received 5 November 2012; accepted 14 March 2013; Published online 11 June 2013
DOI: 10.1002/app.39286

INTRODUCTION

Recently, various supercritical fluid processing methods have been developed for the production of polymer-based materials such as foams, microparticles, membranes and fibers.[1] In this direction, cellular polymers can be formed through the gas foaming technique. Current processes producing microcellular foams include batch, extrusion, injecting molding, extrusion injecting molding, extrusion blow molding, and thermoforming.[2–4] Batch foaming process is one of the most common processes, because it can produce foams with small size and high cell density.[5,6] In general, two batch foaming processes are used to produce foams: temperature-induced and pressure-induced phase separation. For the former one, samples must be put into the oil bath just above the melting point after saturation, the near-surface region melts quickly and stays molten, whereas the interior remains intact, thus leading to nonuniform cells in foams; for the latter one, samples are placed into the high-pressure vessel in the polymer-softening temperature range, which is narrow for many polymers especially polypropylene (PP),[7] any variation in temperature will be enough to make them unfoamed. Huang et al. combined these two processes and developed a new one to foam PP.[8] Although PP foams with small cells and high cell density are achieved, the saturation time is too long (ca. 24 h) and cell morphology is apparently affected by crystalline regions, which makes it difficult to establish model to predict cell morphology of PP.

To reduce the crystalline effect and saturation time, a new foaming process was proposed. First, samples were saturated with supercritical carbon dioxide ($scCO_2$) at high temperature to disrupt crystalline regions completely. Then the temperature was decreased to the foaming one, which was above the crystallization point. Finally, the system was depressurized dramatically to get PP foams. With this new process, PP foams with small cells and high cell density were successfully obtained, the foaming temperature range was largely widened, which could be represented by variations of expansion ratio with foaming temperature.[9] Also, in this new process, the diffusion of CO_2 into PP was quickly due to high kinetic energy of CO_2 and low melt strength of PP matrix at high temperature, thus reducing saturation time obviously. Therefore, the time producing foams was much shorter than that of the pressure-induced or temperature-induced phase separation process.

The classical nucleation theory is widely accepted and used to describe the cell nucleation.[10–12] However, many other researchers indicate that it is not able to fully describe the nucleation activity in the foaming process,[13–15] which is mainly because the pressure inside the cell (P_g) cannot be obtained accurately. To solve this problem, an activation model was established on the basis of previous researches.[16–20] However, the CO_2 solubility need to be accurately obtained in this activation model, which can be calculated according to many theories, such as S-L EOS,[21,22] Simha-Somcynsky (S-S) EOS[23] and perturbed chain

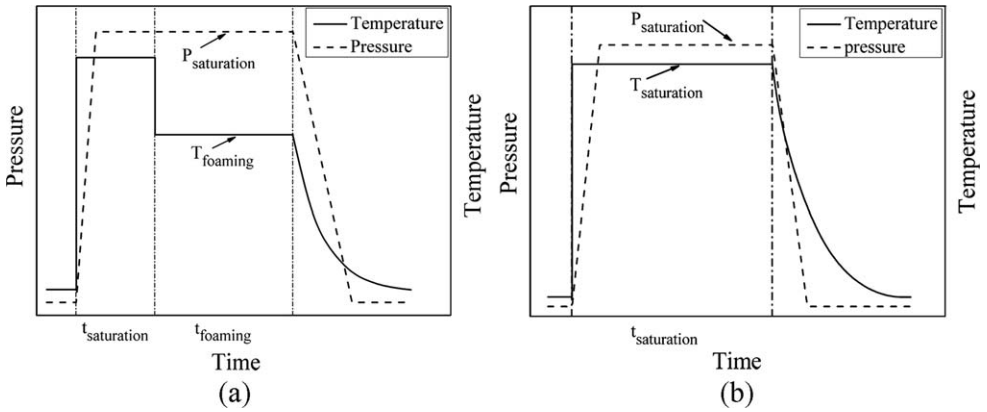

Figure 1. Schematic diagrams of pressure and temperature evolution versus time in the foaming strategy. The processes are: (a) the new process; (b) the conventional process.

statistical associating fluid theory (PC-SAFT) EOS.[24] Among these models, the S-L EOS model is most usually used to describe the P-V-T behavior of many polymer-supercritical fluid systems.[25–29] Therefore, in this article, S-L EOS model was used to calculate the CO_2 solubility. In previous researches, some theories combining with classical nucleation theory and S-L EOS model have been proposed to simulate cell nucleation accurately of amorphous polymers,[30,31] but they can not be used to simulate cell nucleation of semicrystalline polymers like PP. In fact, only few researchers have studied cell nucleation of PP.

In this article, an activation model was established on the basis of the mass equilibrium, and we combined it with classical nucleation theory and S-L EOS model to simulate cell nucleation and cell diameter of PP foams. The experimental value was used to be corrected with this theory. In addition, an improved process was proposed, whose advantages were explored and confirmed by Differential scanning calorimetry (DSC) characterization.

EXPERIMENTAL

Materials

PP pellets (F401) with an average diameter of 3–4 mm were supplied by Sinopec Yangzi Petrochemical Co., Lit., China. The mass-average molar mass was 985,000 g/mol. The CO_2 (purity 99%) was purchased from Nanjing Gas Co. of 55th Institute and used as received.

Preparation of the Porous Structures

In this work, PP was foamed with a batch foaming apparatus as shown in previous report.[9,32] The foaming procedures were as follows: (1) placing samples in the high-pressure vessel with 100 cm^3 internal volume; (2) slowly flushing the vessel with low pressure CO_2; (3) heating the vessel to the temperature of 170°C within 20 min; (4) pressurizing the vessel to the saturation pressure with high-pressure CO_2; (5) saturating samples in the vessel for 30 min at the saturation pressure; (6) declining the temperature to the foaming one within 30 min, remaining the saturation pressure unchanged during temperature declining and then keeping the temperature for 60 min; (7) depressurizing the vessel to the atmospheric pressure in less than 10 s; (8) injecting foamed samples out of the vessel quickly and immersing them into ice-water mixture to stabilize cell nuclei. The whole procedures are shown in Figure 1(a).

The conventional process was mentioned in other article.[7] The whole procedures are shown in Figure 1(b).

Characterization

DSC was conducted on the PP with a Mettler Toledo DSC 823E (Mettler, Switzerland). Weighted sample was sealed in aluminum hermetic pans and heated up to 220°C at a rate of 10°C/min, held at that temperature for 5 min, then cooled to 50°C at a rate of 10°C/min. All measurements were carried out under the CO_2 atmosphere environment. The mass of sample was 10–20 mg.

The surface tension of PP at different temperatures was measured with pendant drop method descried in other articles.[33,34] Samples were molded to 10 × 2 × 2 mm. Then samples were hang in the heating equipment with a window under the CO_2 atmosphere, the sample melting process was recorded with a digital camera.

Foamed samples were immersed in liquid nitrogen for 30 min and then fractured. Fractured surfaces were coated with gold and then examined with the JSM 6380 SEM (Japan Electron Optics Laboratory Co., Ltd., Japan) at an acceleration voltage of 30 kV to observe cellular structures of foamed samples. The average cell diameter was obtained by the software image proplus. The number average diameter of all the cells in the micrograph, D, was calculated with the following equation:[9,32]

$$D = \frac{\sum_{i=2}^{n} d_i}{n}. \quad (1)$$

where n is the number of cells in the micrograph and d_i is the perimeter-equivalent diameter.

The cell density N_c and the expansion ratio R_v in the foam were calculated based on eqs. (2)[32] and (3)[9] in which ρ_f is the foam density, ρ_p is the mass density of PP, both were measured according to ASTMD 792-00:

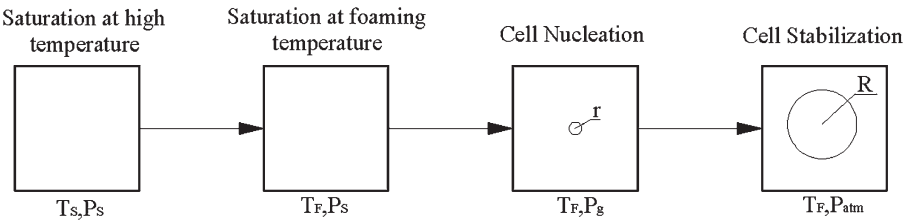

Figure 2. Cell nucleation and stabilization process.

$$N_c = 10^{12} \times \frac{6\left[1-\frac{\rho_f}{\rho_p}\right]}{\pi D^3} \left(\text{cells/cm}^3\right) \quad (2)$$

***

$$R_V = \frac{\rho_p}{\rho_f} \quad (3)$$

THEORY

Nucleation Theory

According to the classical nucleation theory,[31,35] the difference of the free energy (ΔG) can be calculated by the following equation:

$$\Delta G = -\frac{4\pi r^3}{3}\Delta P + 4\pi r^2 \gamma. \quad (4)$$

The critical radius (r_c) and the maximum value of ΔG (ΔG^*_{hom}) are:[31,35]

$$r_c = \frac{2\gamma}{\Delta P} \quad (5)$$

$$\Delta G^*_{\text{hom}} = \frac{16\pi r^3}{3\Delta P^2} \quad (6)$$

$$\Delta P = P_g - P_{atm} \quad (7)$$

The nucleation rate (N_0) and the total number of nuclei (N_c) are[31,35]

$$N_0 = C_0 f_0 \exp\left(\frac{-\Delta G^*_{\text{hom}}}{kT}\right) \quad (8)$$

$$f_0 = ZR_{imp}\left(4\pi r_c^2\right) \quad (9)$$

$$N_c = \int_0^{t,vitr} N_0 dt = \int_{p,sat}^{p,vitr} N_0 \frac{dp}{dp/dt} \quad (10)$$

where r is the radius of the cell, γ is the interfacial tension of polymer melt, ΔP is the pressure difference between two sides of the interface between the nucleus and the mother phase, P_g is the pressure inside the cell, P_{atm} is the atmospherically pressure, C_0 is the concentration of the dissolved fluid inside the polymer matrix, k is the Boltzmann constant, Z is the Zeldovich factor, R_{imp} is the rate of impingement of gas molecules, the parameter f_0 is a frequency factor for gas molecules, the sat and vitr denote saturation and vitrification, respectively.

According to eqs. (4–10), to apply the nucleation theory, the pressure inside cells, the amount of the dissolved fluid and the interfacial tension are required. Consequently, in the absence of extended experimental value there is a need of an appropriate model.

Activation Model

To obtain the pressure inside cells, we combined some well-know cell models,[20,36–38] and an idealized cell nucleation is constructed in Figure 2. The following assumptions are used in this model:

1. The system is isothermal;
2. The cell is spherically symmetric;
3. The polymer melt is incompressible;
4. The inertial forces and gravity are neglected;
5. The gas concentration in the polymer-gas solution and the pressure inside the cell obeys Henry's law. The concentration of CO_2 in the volume of PP from which the cell can draw its gas is symmetric;
6. The volume and mass of PP from which the cell can draw its gas is almost the same for each cell;
7. There is no loss of gas to the surroundings.

With this model, one can write the expression according to mass equilibrium and previous assumptions. The mass of CO_2 in the cell is:

$$m_{bubble} = \frac{4}{3}\pi r^3 \rho_{CO2}\left(T_F, P_g\right) \quad (11)$$

Where $\rho(T_F,P_g)$ is the mass density of CO_2 at the pressure of P_g and the temperature of T_F. For this article, the CO_2 solubility can be obtained:

$$S(T,P) = \frac{m'_{CO2}}{m'_p} \quad (12)$$

Where m'_{CO2} is the mass of CO_2 in the polymer at the weight of m'_p. The gas available in the polymer before the foaming event is:

$$m_{Supply} = S(P_S, T_F)\, m_p \quad (13)$$

Where m_p is the mass of polymer from which the cell can draw its gas.

According to the seventh assumption, the amount of gas remaining in the polymer (m_{polymer}) by subtracting the mass of gas added to the cell (m_{cell}) from the mass of gas initially in the polymer (m_{supply}):

$$m_{polymer} = m_{supply} - m_{cell} \quad (14)$$

According to the definition of the solubility, m_{polymer} can be rewritten to yield:

$$m_{Polymer} = S\left(P_g, T_F\right) m_p \quad (15)$$

According to the fifth assumption, the CO_2 solubility around cells is:

$$S(P_g, T_F) = 0.044 K_h P_g \quad (16)$$

K_h is the Henry's constant, $K_h = 3.0 \times 10^{-7}$ mol·kg^{-1}·Pa^{-1} according to ref. 1.

Finally, eqs. (11), (13), (15) and (16) are substituted into eq. (14) to yield:

$$0.044 K_h P_g m_P = S(P_S, T_F) m_P - \frac{4}{3}\pi r^3 \rho_{CO2}(P_g, T_F) \quad (17)$$

According to the fifth and sixth assumptions, m_p, in this article, can be defined as follows:

$$m_p = \frac{\rho_p}{N_c} = \frac{4\pi r^3}{3}\frac{\rho_p^2}{\rho_p - \rho_f} \quad (18)$$

Substituting eqs. (2) and (17) into eq. (18):

$$\frac{0.044 K_h P_g \rho_P^2}{\rho_P - \rho_f} = \frac{S(P_S, T_F)\rho_P^2}{\rho_P - \rho_f} - \rho_{CO2}(P_g, T_F) \quad (19)$$

This equation is then solved to yield P_g. The solubility and mass density of CO_2 are solved based on S-L EOS model in the next section.

Calculation of Solubility

The densities of CO_2 in the headspace of the autoclave were calculated by BWR.[39] The CO_2 solubility can be calculated by S-L EOS model:[39]

$$S_{CO2} = \left[\frac{m_{CO2} - (V_h + V_{pol}) \times \rho_{CO2}}{m_p} + \frac{\rho_{CO2}}{\rho(T,P)}\right] \times \frac{1000 \times \rho(T,P)}{1000 \times \rho(T,P) - \rho_{CO2}} \quad (20)$$

Where S_{CO2} is the CO_2 solubility in the polymer, ρ_p is the mass density of the polymer, and $\rho(T,P)$ is the mass density of polymer/CO_2 estimated by S-L EOS at each condition. The mass fraction of CO_2 (ω_{CO2}) and polymer (ω_{pol}) are:

$$\omega_{CO2} = \frac{S_{CO2}}{1 + S_{CO2}} \quad (21)$$

$$\omega_{pol} = 1 - \omega_{CO2} \quad (22)$$

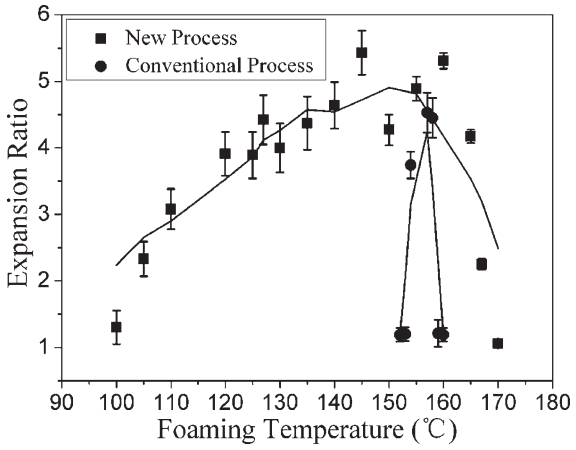

Figure 3. Variations of expansion ratio of PP foams with foaming temperature in the new process. The saturation pressure is 25 MPa.

Calculation of Surface Tension

The interfacial tension was calculated with the following empirical equation:[20]

$$\gamma_{mix} = (1 - \omega_{CO2})^r \gamma_{pol} \quad (23)$$

Where γ_{mix} and γ_{pol} is the surface tension of the mixture and pure polymer, respectively. r is the empirical coefficient.

RESULTS AND DISCUSSION

Advantages of the New Process

Figure 3 shows the foaming temperature range of two processes. Error bars represent the standard deviation for each value of repeated experiments. From Figure 3, the foaming temperature range of the new process is about 12 times broader than that of the conventional one, indicating that the foamability of PP has been largely improved with the new process. At the temperature of 170°C, CO_2 in the PP matrix can get equilibrium within very short time due to the low melt strength of PP and high CO_2 diffusion rate. When the temperature is decreased to the foaming one, the PP matrix remains low melt strength, which is easy for CO_2 to reach equilibrium again, the time producing foams is decreased to 2.5 h, which is the shortest in batch foaming

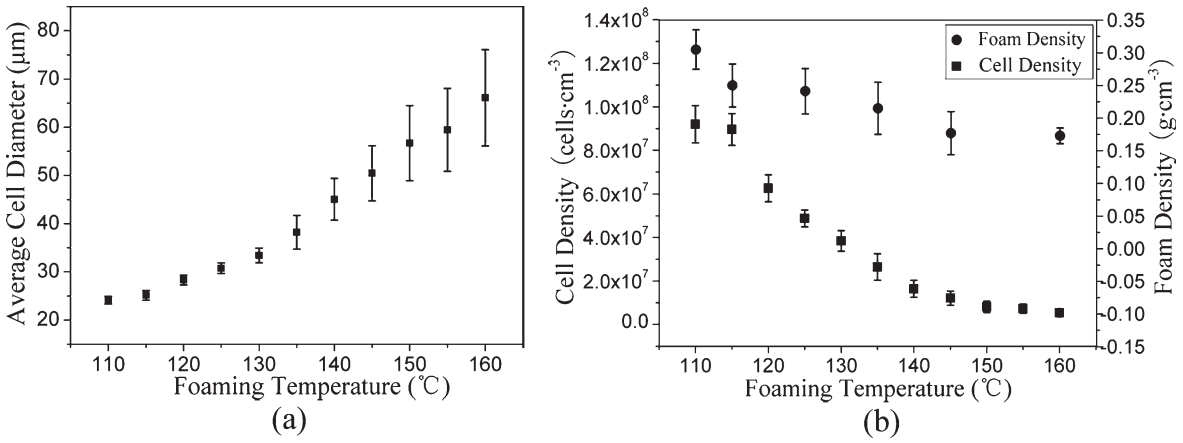

Figure 4. Variations of the cell diameter, cell density and foam density of PP foams with foaming temperature in the new process. The saturation pressure is 25 MPa.

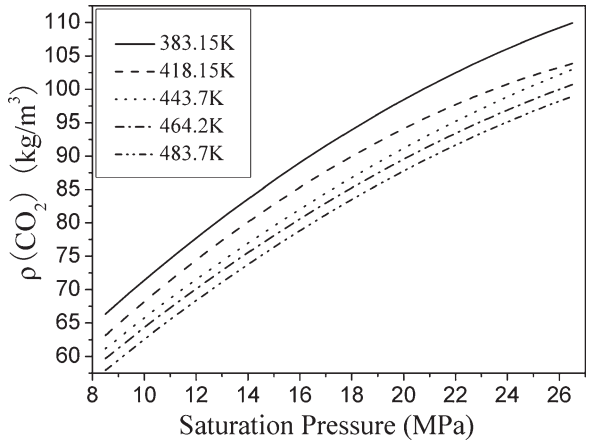

Figure 5. Variations of the mass density of CO_2 with saturation pressure at different temperatures.

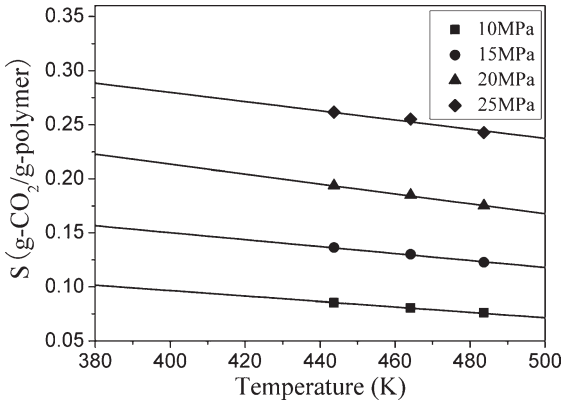

Figure 7. Solubility of CO_2 in molten state PP at different pressures. Experimental results (symbols)[45] and calculation results (lines) via S-L EOS with $k_{12} = 5.45–0.0365T$.

processes as far as we know. As previous articles reported that if PP matrix melted, it would become hard at very low temperature.[40,41] Therefore, the lower limit of foaming temperature declines. In the conventional process, PP begins to be foamed at the near-melting temperature, thus increasing the lower limit of foaming temperature.

The upper limit of foaming temperature for the new process should be the same as that for the conventional one. However, the phenomenon we observed is different, which needs to be further investigated in the near future.

Effect of Foaming Temperature

Figure 4 shows variations of the cell diameter, cell density and foam density with the foaming temperature at the saturation pressure of 25 MPa. As presented in this figure, the cell diameter increases, whereas the foam density and cell density decrease with foaming temperature rising. Error bars in Figure 4(a,b), respectively represent the standard deviation for the size and the cell density of each cell, which is calculated by substituting each cell size into eq. (2). According to eq. (19), under constant saturation pressure, P_g can be solved as follows:

$$P_g = \frac{S(P_S, T_F)}{0.044K_h} - \frac{\rho_{CO2}(P_g, T_F)\left(\rho_P - \rho_f\right)}{0.044\rho_P^2} \tag{24}$$

ρ_p is about 939 kg·m^{-3}, ρ_f is more than 150 kg·m^{-3}, K_h is 3.0×10^{-7} kg·mol^{-1}·Pa^{-1}. The precoefficients of $S(T_F,P_S)$ and $\rho_{CO2}(P_g,T_F)$ are estimated as 7.58×10^7 kg·mol^{-1}·Pa^{-1} and 0.02 kg·m^{-3}, respectively. The variation of ρ_{CO2} with the temperature remains small although the pressure or temperature varies apparently as shown in Figure 5. Therefore, $\rho_{CO2}(P_g,T_F)$ almost has no effect on P_g comparing with the $S(P_S,T_F)$.

According to eq. (4), ΔG increases with increase of γ and decrease of ΔP. The γ of PP melt decreases with the temperature rising as shown in Figure 6(a). Nevertheless, as predicted from eq. (23), this happens only at low pressures, where the CO_2 solution is not very high. At high pressures the decrease of the CO_2 solubility caused by the temperature increase is pronounced and γ increases with the temperature rising as shown in Figure 6(b), which is the same as the results of refs. 33,34, and 44. The CO_2 solubility in the PP decreases with temperature rising and almost shows linear relationship as

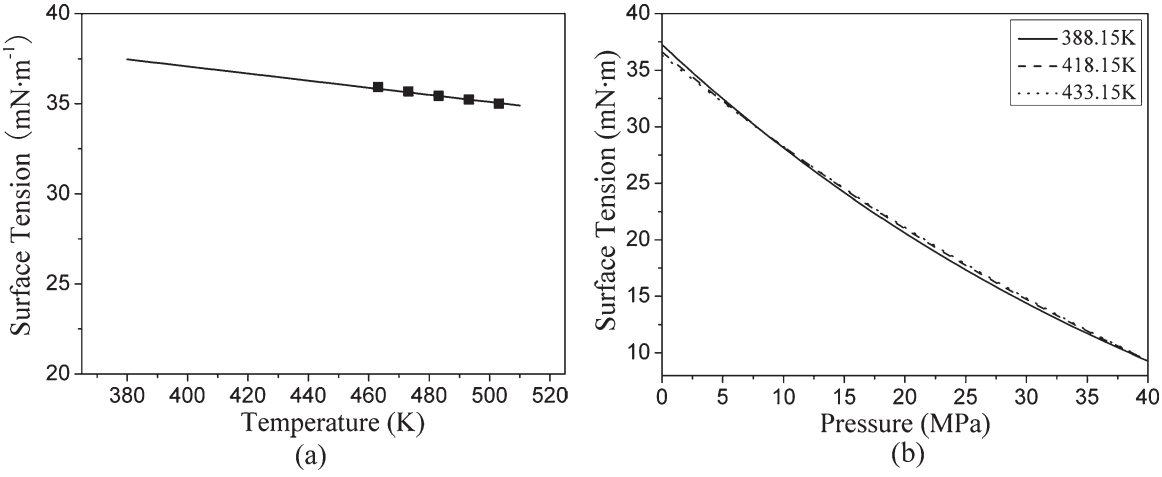

Figure 6. Variations of surface tension of PP melt with temperature at (a) atmosphere pressure and (b) different pressures: Experimental results (symbols) and calculation results (lines).

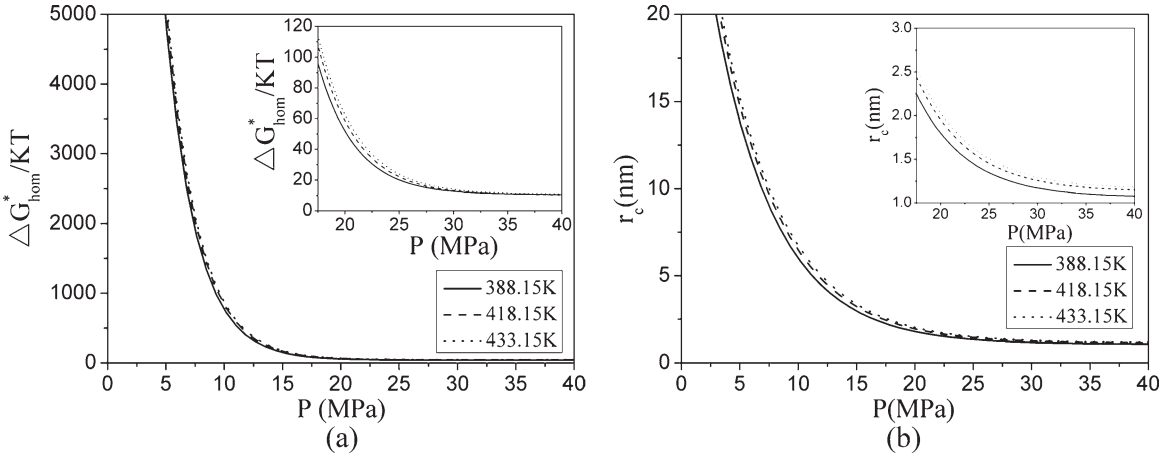

Figure 8. Energy barrier and critical nucleus for homogeneous nucleation in the PP-CO_2 system.

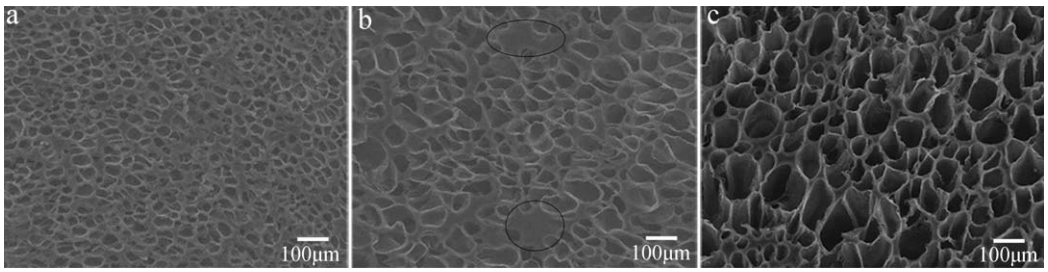

Figure 9. SEM micrographs of PP foams at different foaming temperatures. The foaming temperatures are (a) 120°C, (b) 135°C, (c) 150°C. The saturation pressure is 25 MPa.

shown in Figure 7, other articles also have reported the same results.[41–43] According to eq. (24), P_g decreases with foaming temperature rising. Therefore, ΔG and r_c increase with foaming temperature rising according to eq. (4) and eq. (5) as shown in Figure 8. Therefore, fewer cells can be nucleated in a given volume at higher foaming temperature, thus leading to lower cell density and larger cells with reduced bulk density.

Figure 9 shows SEM micrographs of PP at different foaming temperatures. It can be found that low temperature leads to small and uniform cells, whereas high temperature results in large and irregular cells. At high temperature, cell coalescence becomes apparent because of the low melt strength, thus leading to large and irregular cells. Some unfoamed regions are observed at the temperature of 135°C as shown in circles in Figure 9(b), but this phenomenon could not be found at the temperature of 150°C. As we know, high temperature benefits both gas diffusion and cell coalescence. Maybe at the temperature of 135°C, gas diffusion plays the dominant role, gas diffuses into surrounding cells, resulting in unfoamed regions. Although at the temperature of 150°C, cell coalescence leads to all regions being foamed.

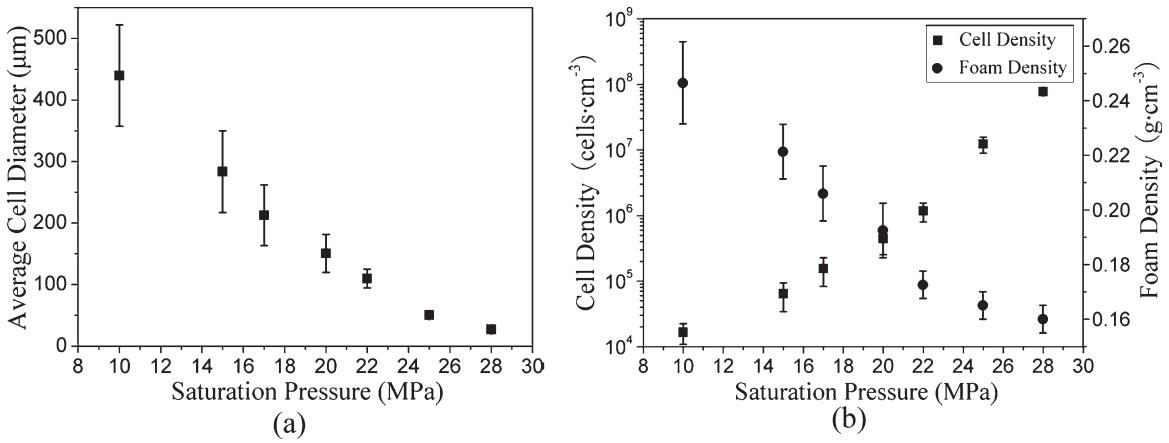

Figure 10. Variations of cell diameter, cell density and foam density of PP foams with saturation pressure. The foaming temperature is 145°C.

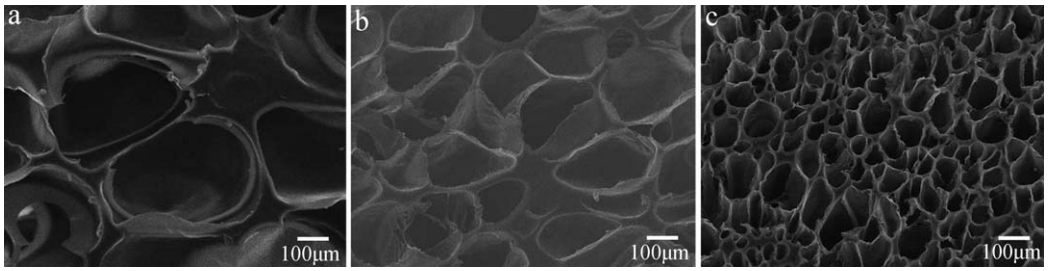

Figure 11. SEM micrographs of PP foams at different saturation pressures. The saturation pressures are (a) 15 MPa, (b) 20 MPa, (c) 25 MPa. The foaming temperature is 145°C.

Table I. Characteristic Parameters for S-L EOS[34]

Substance	T*, K	P*, MPa	ρ^*, kg/m^3	M_i, g/mol	T, K	P, MPa	Ref.
CO_2	300	630	1515	44			36
PP	692	297.5	882.8	197,000	303-589	0-200	13

Effect of Saturation Pressure

Figure 10 shows variations of the cell diameter, cell density and foam density with the saturation pressure. The cell diameter and foam density decrease, whereas the cell density increases with increase of saturation pressure. This is caused by the increase of P_g and the decrease of γ_{mix}. $S(P_S,T_F)$ increases with increase of saturation pressure as shown in Figure 7, other articles have also got the same results.[40,41,44] According to

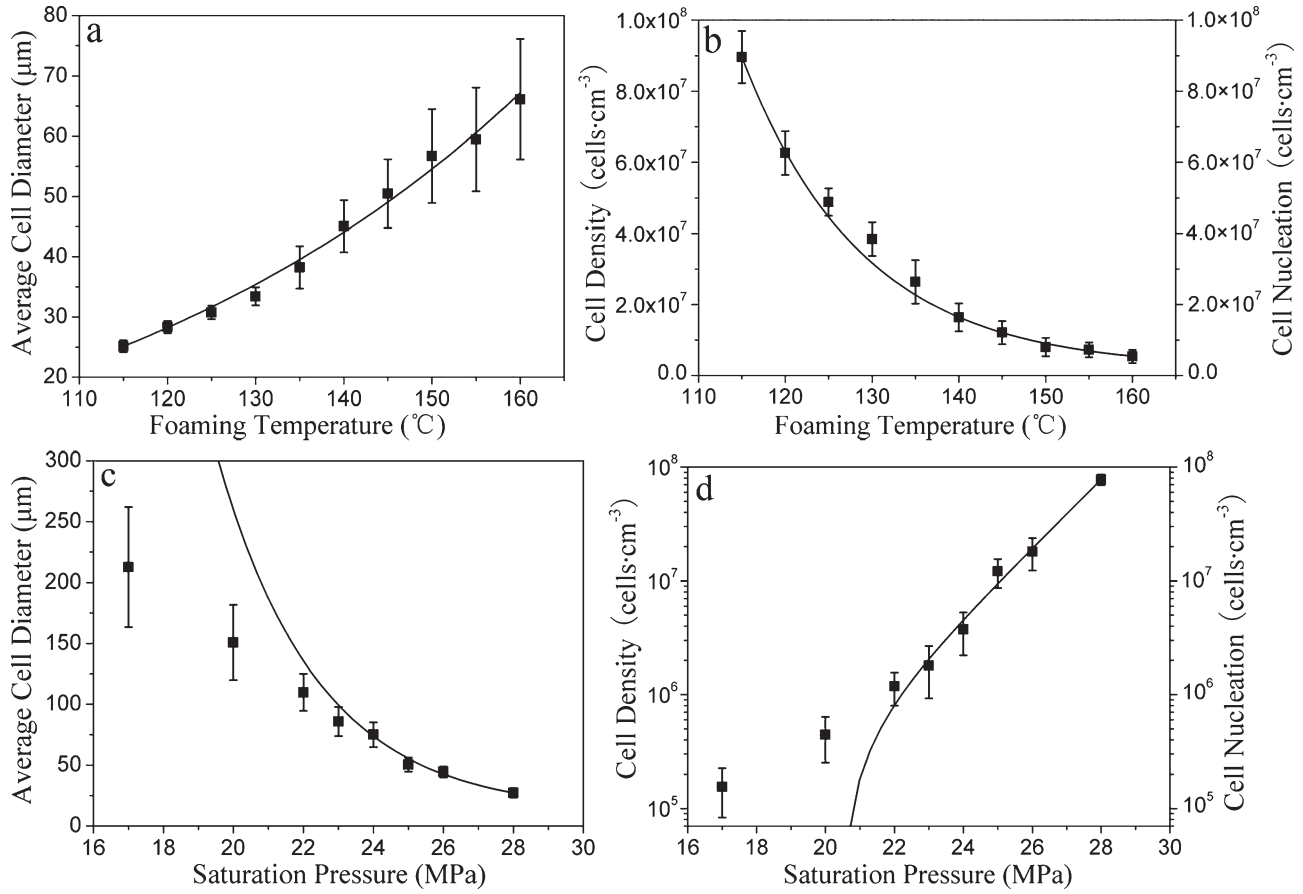

Figure 12. Variations of average cell diameter and cell density of PP foams with foaming temperature at the saturation pressure of 25 MPa and saturation pressure at the foaming temperature of 145°C. Cell density (symbols) and cell nucleation (lines).

eq. (24), under constant foaming temperature, P_g increases with increase of $S(P_S,T_F)$, thus leading to the decrease of ΔG and r_c. Higher $S(P_S,T_F)$ leads to larger ω_{CO2}, which results samller γ_{mix} as shown in Figure 6(b), ΔG and r_c further decrease according to eqs. (4) and (5). Therefore, ΔG and r_c decreases with increase of saturation pressure as shown in Figure 8. More cells can be nucleated in a given volume at higher saturation pressure, small cells and high cell density are produced.

Figure 11 shows SEM micrographs of PP at different saturation pressures. At low saturation pressure, large and discrete cells appear in PP foams, unfoamed regions are apparently observed, whereas at high saturation pressure, small and combining cells are found. This is because low pressure leads to low CO_2 solubility and low cell nucleation, but the CO_2 diffusion is high because of the low melt strength after high temperature treatment, unfoamed regions are formed.

Theoretical Corrections

According to eq. (23), the parameter r was estimated to be 3 by fitting the experimental value from other ref. 45, as shown in Figure 6(b). In this article, PP was first melted at high temperature and then the temperature was decreased to the foaming one, which was lower than the melting temperature. Because the CO_2 solution without crystalline regions at low temperature could not be found in other articles, so it only could be calculated with S-L EOS model. The results are illustrated in Figure 6. The S-L EOS pure fluid scaling parameters are presented in Table I.[34]

In this study, the nucleation theory, combines with the activation model and S-L EOS model, is used to predict both the cell nucleation and cell diameter of PP foams, ZR_{imp} is used as a fitted parameter. Results are summarized in Figure 12. As observed, a good agreement between experimental and calculated values is obtained. However, we have observed some limited nucleation activity at saturation pressures as low as 20 MPa, a phenomenon that is not predicted by this theory. This may be because of the limitation of Henry's law and the fifth assumption is not successful at low pressure. It can be found from Figure 12 that large unfoamed regions are apparently observed at low pressure, which means the volume of PP from which the cell can draw its gas is very large and the CO_2 concentration is not symmetric. However, in Figure 9, these phenomena are not found at different foaming temperatures.

CONCLUSIONS

In this work, a new process was used to produce PP foams with $scCO_2$ as the blowing agent. Results revealed that the foaming temperature range was 12 times broader than that of the conventional one and the time producing foams was only 2.5 h. The cell diameter decreased and the cell density increased with increase of saturation pressure, or decrease of foaming temperature.

The results were corrected by classical nucleation theory combining with S-L EOS and activation model, which was established on the basis of the mass equilibrium. A satisfactory agreement between corrections and experimental values was obtained indicating that this activation theory could accurately simulate the cell nucleation and cell diameter of PP. In addition, this model was used to explain foaming behaviors of PP.

ACKNOWLEDGMENTS

This work was supported by Independent Research and Special Programs of Nanjing University of Science and Technology (Grant No. 2010ZYTS018) in 2011.

REFERENCES

1. Tomasko, D. L.; Li, H.; Liu, D.; Han, X.; Wingert, M. J.; Lee, J.; Koelling, K. W. *Ind. Eng. Chem. Res.* **2003**, *42*, 6431.
2. Ruiz, J. A. R.; Viot, P.; Dumon, M. *J. Appl. Polym. Sci.* **2010**, *118*, 320.
3. Zhang, P.; Wng, X. J.; Yang, Y.; Zhou, N. Q. *J. Appl. Polym. Sci.* **2009**, *114*, 1320.
4. Tomasko, D. L.; Burley, A.; Feng, L.; Yeh, S. K.; Miyazono, K. *J of Supercrit Fluids* **2009**, *47*, 493.
5. Famili, M. H. N.; Janani, H.; Enayati, M. S. *J. Appl. Polym. Sci.* **2011**, *119*, 2847.
6. Sharudin, R. W.; Nabil, A.; Taki, A.; Taki, K.; Ohshima, M. *J. Appl. Polym. Sci.* **2011**, *119*, 1042.
7. Xu, Z. M.; Jiang, X. L.; Liu, T.; Hu, G. H.; Zhao, L.; Zhu, Z. N.; Yan, W. K. *J Supercrit Fluids* **2007**, *41*, 299.
8. Huang, H. X.; Wang, J. K. *J. Appl. Polym. Sci.* **2007**, *106*, 505.
9. Ding, J.; Shangguan, J. N.; Ma, W. H.; Zhong, Q. *J. Appl. Polym. Sci.* **2012**, DOI: 10.1002/APP.38416.
10. Kim, S. G.; Lee, J. W. S.; Park, C. B.; Sain, M. *J. Appl. Polym. Sci.* **2010**, *118*, 1691.
11. Leung, S. N.; Li, H. B.; Park, C. B. *J. Appl. Polym. Sci.* **2007**, *104*, 906.
12. Sun, X. H.; Liu, H. J.; Li, G.; Liao, X.; He, J. S. *J. Appl. Polym. Sci.* **2004**, *93*, 163.
13. Naguib, H. E.; Park, C. B.; Reichelt, N. *J. Appl. Polym. Sci.* **2004**, *91*, 2661.
14. Guo, Z. H.; Burley, A. C.; Koelling, K. W.; Kusaka, I.; Lee, J.; David, L. *J. Appl. Polym. Sci.* **2012**, *125*, 2170.
15. Li, Y.; Yao, Z.; Chen, Z. H.; Cao, K.; Qiu, S. L.; Zhu, F. J.; Zeng, C. C.; Huang, Z. M. *Chem. Eng. Sci.* **2011**, *66*, 3656.
16. Kumar, V.; Suh, N. P. *Polym. Eng. Sci.* **1990**, *30*, 1323.
17. Kim, Y. Y.; Park, C. B.; Chen, P.; Thompson, R. B. *Polymer* **2011**, *52*, 5622.
18. Zhang, P.; Wang, X. J.; Yang, Y.; Zhou, N. Q. *J. Appl. Polym. Sci.* **2010**, *118*, 1949.
19. Wong, A.; Chu, R. K. M.; Leung, S. N.; Park, C. B.; Zong, J. H. *Chem. Eng. Sci.* **2011**, *66*, 55.
20. Cloton, J. S. The Nucleation of Microcellular Thermoplastic Foams. Dissertation for the Doctoral Degree, Massachusetts Institute of Technology, Department of Chemical Engineering, Massachusetts, **1986**.
21. Isaac, C. S.; Robert, H. L. *J. Phys. Chem.* **1976**, *80*, 2352.
22. Isaac, C. S.; Robert, H. L. *Macromolecules* **1978**, *11*, 1145.

23. Simha, R.; Somcynsky, T. *Macromolecules* **1969**, *2*, 342.
24. Huang, S. H.; Radosz, M. *Ind. Eng. Chem. Res.* **1991**, *30*, 1994.
25. High, M. S.; Danner, R. P. *AIChE J.* **1990**, *36*, 1625.
26. Lee, B. C.; Danner, R. P. *AIChE J.* **1996**, *42*, 837.
27. Byung-Chul, L.; Danner, R. P. *Fluid Phase Equilib* **1996**, *117*, 33.
28. Danner, R. P.; Hamedi, M.; Lee, B. C. *Fluid Phase Equilib* **2002**, *194*, 619.
29. Hamedi, M.; Muralidharan, V.; Lee, B. C.; Danner, R. P. *Fluid Phase Equilib* **2003**, *204*, 41.
30. Tsivintzelis, I.; Angelopoulou, A. G.; Panayiotou, C. *Polymer* **2007**, *48*, 5928.
31. Gabbard RG, The development of a homogeneous nucleation rate model for the thermoplastic foams based on a molecular partition function and fickian diffusion. Dissertation for the Doctoral Degree, New Jersey Institute of Technology, Department of Chemical Engineering, New Jersey, **2002**.
32. Ding, J.; Ma, W. H.; Zhong, Q. *Polym-Plast. Technol. Eng.* **2012**, *52*, 7.
33. Moreira, C. J.; Demarquette, N. R. *J App Polym. Sci.* **2001**, *82*, 1907.
34. Park, H.; Park, C. B.; Tzoganakis, C.; Tan, K. H.; Chen, P. *Ind. Eng. Chem. Res.* **2006**, *45*, 1650.
35. Goel, S. K.; Beckman, E. *J. Polym. Eng. Sci.* **1994**, *34*, 1137.
36. Leung, S. N.; Park, C. B.; Xu, D.; Li, H.; Fenton, R. G. *Ind. Eng. Chem. Res.* **2006**, *45*, 7823.
37. Tuladhar, T. R.; Mackley, M. R. *Chem. Eng. Sci.* **2004**, *59*, 5997.
38. Kweeder, J. A. Nucleation mechanisms in microcellular polymer foams. Dissertation for the Doctoral Degree, Clarkson University, Department of Chemical Engineering: New York, **1997**.
39. Li, D. C.; Liu, T.; Zhao, L.; Yuan, W. K. *Ind. Eng. Chem. Res.* **2009**, *48*, 7117.
40. Ding, J.; Ma, W. H.; Song, F. J.; Zhong, Q. *J. Mater. Sci.*, DOI: 10.1007/s10853-012-7039-1.
41. *Polymer* **2000**, *41*, 1011.
42. Sato, Y.; Fujiwara, K.; Takilkawa, T.; Sumarno; Takisima, S.; Masuoka, H. *Fluid Phase Equilib* **1999**, *162*, 261.
43. Li, G.; Gunkel, F.; Wang, J.; Park, C. B.; Altstadt, V. *J. Appl. Polym. Sci.* **2007**, *103*, 2945.
44. Lei, Z. G.; Ohyabu, H.; Sato, Y.; Inomata, H.; Richard, L. S. *J. J Supercrit Fluids* **2007**, *40*, 452.
45. Markocic, E.; Skerget, M.; Zeljko, K. *J Supercrit Fluids* **2011**, *55*, 1046.